


Label-Free Characterization and Quantification of Mucosal Inflammation in Common Murine Colitis Models With Multiphoton Imaging

Lucas Kreiss, Dr.-Ing,^{*,†,‡,§,¶,||}  Oana-Maria Thoma, Dr. rer. nat,^{*,†,‡,§,¶} Sarah Lemire,^{*,§} Kristina Lechner, MSc,^{*,§} Birgitta Carlé, MSc,[†] Ashwathama Dilipkumar, MSc,^{†,‡} Timo Kunert, MSc,^{*,§} Kristina Scheibe, Dr. rer. nat,^{*,§} Christina Heichler, MSc,^{*,§} Anna-Lena Merten, MSc,^{†,‡} Benno Weigmann, PD Dr. rer. nat,^{*,§} Clemens Neufert, PD Dr. med,^{*,§} Kai Hildner, Prof. Dr. med,^{*,§} Michael Vieth, Prof. Dr. med,^{¶,||} Markus F. Neurath, Prof. Dr. med,^{*,§} Oliver Friedrich, Prof. Dr. med, Dr. rer. nat,^{†,‡} Sebastian Schürmann, Dr. rer. nat,^{†,‡,¶,||} and Maximilian J. Waldner, Prof. Dr. med,^{*,†,‡,§,¶,||}

From the *Department of Medicine 1, University Hospital Erlangen, Friedrich-Alexander University Erlangen-Nürnberg, Erlangen, Germany

[†]Institute of Medical Biotechnology, Friedrich-Alexander University Erlangen-Nürnberg, Erlangen, Germany

[‡]Erlangen Graduate School in Advanced Optical Technologies, Friedrich-Alexander University Erlangen-Nürnberg, Erlangen, Germany

[§]Deutsches Zentrum Immuntherapie, Erlangen, Germany

[¶]Institute of Pathology, Klinikum Bayreuth, Bayreuth, Germany

^{||}Institute of Pathology, University Hospital Erlangen, Friedrich-Alexander University Erlangen-Nürnberg, Erlangen, Germany.

^{*}These authors contributed equally as co-first authors.

[¶]These authors contributed equally as co-senior authors.

Address correspondence to: Lucas Kreiss, Dr.-Ing, Institute of Medical Biotechnology, Paul-Gordan-Str 3, 91052 Erlangen, Germany (Lucas.Kreiss@fau.de).

Background: Clinical challenges in inflammatory bowel diseases require microscopic in vivo evaluation of inflammation. Here, label-free imaging holds great potential, and recently, our group demonstrated the advantage of using in vivo multiphoton endomicroscopy for longitudinal animal studies. This article extends our previous work by in-depth analysis of label-free tissue features in common colitis models quantified by the multiphoton colitis score (MCS).

Methods: Fresh mucosal tissues were evaluated from acute and chronic dextran sulfate sodium (DSS), TNBS, oxazolone, and transfer colitis. Label-free imaging was performed by using second harmonic generation and natural autofluorescence. Morphological changes in mucosal crypts, collagen fibers, and cellularity in the stroma were analyzed and graded.

Results: Our approach discriminated between healthy (mean MCS = 2.5) and inflamed tissue (mean MCS > 5) in all models, and the MCS was validated by hematoxylin and eosin scoring of the same samples (85.2% agreement). Moreover, specific characteristics of each phenotype were identified. While TNBS, oxazolone, and transfer colitis showed high cellularity in stroma, epithelial damage seemed specific for chronic, acute DSS and transfer colitis. Crypt deformations were mostly observed in acute DSS.

Conclusions: Quantification of label-free imaging is promising for in vivo endoscopy. In the future, this could be valuable for monitoring of inflammatory pathways in murine models, which is highly relevant for the development of new inflammatory bowel disease therapeutics.

Key Words: Multiphoton Microscopy, Experimental Colitis, Label-free Imaging

Introduction

Lately, advanced optical technologies for in vivo diagnostics have refined endoscopy and support conventional histology in preclinical and clinical applications. While confocal laser scanning endoscopy (CLE) is based on exogenous fluorescent contrast agents,¹⁻³ multiphoton microscopy (MPM) allows label-free imaging of native proteins, such as nicotinamide adenine dinucleotide (NADH), flavin adenine dinucleotide (FAD), and collagen.⁴ Therefore, MPM has the advantages of natural 3-dimensional (3D) contrast and enhanced optical penetration depth. The label-free contrast mechanisms of MPM have led to developments in multiphoton endomicroscopy

(MPM).⁵⁻¹¹ In the context of preclinical studies, this allows longitudinal in vivo studies of tissue microstructure in the same animals over the time course of experimental colitis models.¹² In the future, label-free endomicroscopy could allow continuous disease monitoring, leading to a faster diagnosis of clinical inflammatory bowel disease (IBD). In the present study, we quantify disease activity in several different experimental colitis models using label-free multiphoton imaging from fresh, ex vivo tissue samples. We developed a reliable diagnostic tool for the quantification of various aspects of inflammatory tissue remodeling in the colon. Furthermore, we used this method for the identification of characteristic

Key Messages

- It is already known that label-free multiphoton microscopy can image native colon tissue, without sectioning or staining.
- Here, we present a systematic quantification of label-free tissue features, leading to comparison of different pathways of inflammatory remodeling in the most common experimental colitis models.
- Because endoscopic applications are already reported and used in preclinical trials, a systematic quantification is an essential asset for future label-free microscopic diagnosis of inflammatory bowel disease patients.

differences in the disease pattern between these models. In the future, label-free MPM can be a valuable tool for detailed monitoring of many disease parameters in murine studies. In the long term, the potential of label-free multiphoton imaging for in vivo applications could lead to a faster diagnosis of clinical IBD as well as to continuous disease monitoring based on label-free, in vivo histology.

Methods

In brief, we used fresh and native tissue samples from 5 different colitis models as well as from 2 healthy control groups. Three-dimensional image stacks from MPM were first recorded and then scored by the novel multiphoton colitis score (MCS).¹³ Adjacent tissue samples were collected from all models and prepared for hematoxylin and eosin (H&E) staining. H&E images from the same animals were then histologically scored by an experienced pathologist.

Experimental Colitis Models

All animal experiments were performed according to the guidelines of the Institutional Animal Care and Use Committee of the State Government of Middle Franconia. Wild-type C57BL/6J (B6/J) male mice were used as healthy control animals and for the acute and chronic dextran sulfate sodium (DSS) models as well as for the acute TNBS and oxazolone colitis models. The transfer colitis model was performed using female immune-deficient Rag1^{-/-} mice, with a B6/J background. For naïve CD4⁺CD25⁻ T cell transfer, female B6/J mice were used as donor animals. As a control model for the transfer colitis model, colon tissue samples from healthy Rag1^{-/-} females were also imaged. All animals were 8 to 12 weeks old and weighed at least 18 to 20 g. In total, 36 animals were used as control animals and for colitis models (see [Supplementary Table 1](#)).

Sample preparation

In each model, tissue samples from the most distal 1.5 cm of the colon were collected and flushed with phosphate-buffered saline to remove remaining stool. This colon section refers to the same region that is accessible by our MPEM system.¹⁴ After tissue removal, samples were investigated by white light stereomicroscopy before MPM imaging to make sure that no accidental damage or stool was observed. These samples were kept in ice-cold phosphate-buffered saline until ex vivo investigation by label-free MPM, followed by scoring using the MCS. An adjacent colon tissue sample was collected for

histopathological analysis via H&E staining. An overview of the number of animals and number of analyzed MPM image stacks is displayed in [Supplementary Table 1](#), the experimental colitis models are shown in [Supplementary Figure 1](#). In each colitis model, the severity of intestinal inflammation was regularly checked by monitoring the body weight and by conventional endoscopy.

C57BL/6J (B6/J) control animals

As control animals, 5 wildtype animals (male, 8-12 weeks old, ~20 g) with C57BL/6J background were analyzed by endoscopy, then sacrificed and imaged by MPM and histopathology prior to the initiation of the colitis models described subsequently. From each animal, 3 tissue segments were extracted to allow analysis of variability between different segments (see Variability of the MCS Across Different Time Points, Different Observers, and Different Tissue Segments).

Rag1^{-/-} control animals

A second control group consisting of 4 immune-deficient Rag1^{-/-} mice with a B6/J background (female, 13 weeks old, ~20 g) was used to establish a valid comparison for the transfer colitis model (see the following), as well as to compare with healthy B6/J animals.

Acute DSS model

For the DSS colitis murine model,¹⁵ 4 wild-type mice with B6/J background (males, age 10 weeks, ~20 g) were subjected to 2% DSS (MP Biomedicals) in drinking water for 9 days. On day 9 of the model, the mice were sacrificed to evaluate the inflammation via MPM. From each animal, 3 tissue segments were extracted to allow analysis of variability between different segments (see section 1e below).

Chronic DSS model

Repeated use of DSS was used to induce chronic colitis in B6/J mice (n = 4, males, 13 weeks old, ~25 g).¹⁵ The chronic DSS model was performed as previously described.¹⁶ In brief, mice received 3 cycles of oral treatment with 2% DSS (MP Biomedicals) via drinking water. Mice were sacrificed on day 70 of the experiment and the colon was collected for multiphoton and H&E evaluation.

Acute TNBS colitis model

The TNBS model was used to describe immune cell-driven inflammation.¹⁷ B6/J mice (n = 4 males and 2 females, age 10 weeks, ~25 g) were first presensitized by using a dose of 5% TNBS diluted in 4 parts acetone (Roth) and 1 part olive oil (Sigma-Aldrich). Prior to applying the TNBS, the mice were anesthetized by using a small dose (~100 µL) of ketamine (12 mg/mL)/xylazine (1.6 mg/mL) solution. Once the mice were anesthetized, a 1.5 × 1.5 cm portion of their abdomen was shaved (with Aesculap animal clipper) and 100-µL TNBS solution was applied to the skin. To ensure full TNBS absorption, B6/J mice were placed in the cage with their abdomen up until awakening. During this time, their temperature was maintained at normal levels by using an infrared lamp. After 5 days, the mice were anesthetized as previously described, and 100 µL of a 2.5% TNBS solution diluted in 100% ethanol (Roth) was applied into their colon. The procedure was performed by carefully inserting a 3.5F catheter (Cetofix Mono 330) 4 cm into

the colon and slow administration of the TNBS solution. After catheter removal, the mice were kept in a vertical position for 60 seconds to ensure full absorption of TNBS and then placed back into the cage under infrared light until awakening.

Acute oxazolone colitis model

Oxazolone-induced acute colitis^{18,19} was induced as following: first, B6/J mice ($n = 8$ mice, 10 weeks old, ~ 20 g) were sensitized by using a 3% oxazolone (4-ethoxymethylene-2-phenyl-oxazolin-5-one, Sigma Aldrich) diluted in 4 parts of acetone (Roth) and 1 part olive oil (Sigma Aldrich). The mice were anesthetized with a small dose (~ 100 μ L) of ketamine (12 mg/mL)/xylazine (1.6 mg/mL) solution. Once anesthetized, 100 μ L of oxazolone solution was applied to their shaved abdomens. The mice were kept on their backs until they woke up to ensure complete oxazolone absorption. Seven days later, the mice were again anesthetized using ketamine/xylazine solution and challenged by using 0.5% to 1% oxazolone solution diluted in 1 part 100% ethanol (Roth) and 1 part H₂O. The solution was applied rectally by using a 3.5F catheter (Cetofix Mono 330) 4 cm into the colon. To prevent the oxazolone from leaking, the mice were positioned with rectum facing upward until awakening.

Transfer colitis model

For the immune cell-driven chronic inflammation, a CD4⁺CD25⁻ T cell transfer colitis model was used in immune-deficient Rag1^{-/-} mice with a B6/J background²⁰ ($n = 5$ females, age 11 weeks, 18–20 g). Naïve CD4⁺CD25⁻ T cells were isolated from the spleens of B6/J mice ($n = 1$ female, age 11 weeks) by using the CD4⁺ Isolation kit and CD25 MicroBead Kit (Miltenyi Biotec). The purity of the cells was assessed at $\geq 95\%$. The freshly isolated CD4⁺CD25⁻ T cells were then injected intraperitoneally at a concentration of 10^6 cells/200 μ L of PBS (Sigma Aldrich).

Conventional Imaging

Histology

After the animals were sacrificed, adjacent colon tissue to the one used for MPM was preserved in Roti-Histofix (Carl Roth) and embedded in paraffin. Afterward, tissue samples were cooled at -20°C , and 3- μ m slices were cut with a microtome (Leica) and collected on glass slides. The slides were then placed in an incubator at 65°C for at least an hour for the paraffin to melt and allow the tissue binding to the slide. The samples were then deparaffinized in Rotihistol (Carl Roth) and rehydrated in 100%, 96%, and 70% ethanol. Further, they were shortly washed in water and the cell nuclei were stained in Harris hematoxylin solution (Carl Roth). Counterstaining of cytoplasm was done by immersing the samples in eosin staining solution (Merck). The cuts were then dehydrated in 70%, 96%, and 100% ethanol. To complete the tissue dehydration, the slides were immersed in Rotihistol and mounted with Entellan mounting medium (Sigma Aldrich). The H&E stainings were then evaluated with the DMi4000B inverse microscope (Leica) at 10 \times and 20 \times magnification. Thus, the field of view in 2-dimensional H&E images was larger compared with the 3D stacks of MPM (25 \times , see the following).

Label-Free MPM

Samples were extracted, transported on ice-cold phosphate-buffered saline and directly imaged using an upright multiphoton microscope (TriMScope II; LaVision BioTec). A mode-locked fs-pulsed Ti:Sa laser (Chameleon Vision II; Coherent) was used for excitation, operating at 810 nm wavelength, with an average laser power at the sample of around 144 mW, a pulse duration of 150 fs, and a repetition rate of 80 MHz. Samples were placed between 2 cover glass slips and in phosphate-buffered saline (PBS) immersion. 3D MPM-image stacks were recorded with a 25 \times water immersion objective (HC Fluotar L 25 \times /0.95 W VISIR, corrected for cover slips; Leica Microsystems). The backscattered signal was collected via the same objective and separated by 2 dichroic beam splitters (ZT405 RDC and T495 LPXR; Chroma). As shown in [Figure 1A](#) and [1B](#), the second harmonic generation (SHG) signal was detected at 405 nm (ET405/20, Chroma), the NADH autofluorescence channel was measured at 450 nm (450/70 BrightLine HC; Semrock Inc) and the one from FAD at 560 nm, respectively (ET 560/40M; Chroma). Images were recorded at $400 \times 400 \mu\text{m}^2$ separated into 512×512 pixels, using 2-fold line averaging and a line speed of 1000 Hz. Axial scanning was performed in a range of 100 to 150 μ m depth at 2- μ m axial spacing to record 3D image stacks. The system was controlled by the ImSpector Pro software (v 5.0.233.0; LaVision BioTec) and images were saved in the bioformat data format (.ome.tif, GNU public license, University of Dundee and Open Microscopy Environment).²¹ Axial adaptation of the laser power or adaptive optics was not used but could be promising prospects to yield higher signal-to-noise ratios at larger tissue depths in the future. A total of 4 to 5 3D stacks were recorded from each sample to calculate reliable mean values of the MCS per sample (see the following). All MPM recording from a single sample required around 30 to 40 minutes under the stated measurements conditions. In this fashion, multiple samples from the same model have been imaged in 1 day. Typically, the total time between tissue extraction and measurement of each sample was 3 to 5 hours, never exceeding 8 hours. X-Z and Y-Z projections were generated using Fiji, after decreasing the axial spacing by bilinear interpolation to obtain cubic voxels (see [Figure 2](#)).

Quantification of Disease Activity via the MCS

A novel scoring system was used for the systematic quantification of label-free multiphoton images. This MCS is divided into 6 different categories that are quantified in 1 of 4 possible grades (0–3). Thereby, the total MCS ranges between 0 and 18. Definitions of the scoring categories are presented in [Table 1](#) and in [Supplementary Figure 1](#). The categories A and B consider the lamina propria and define shape (category A) as well as size and distance of mucosal crypts (category B), based on the autofluorescence in the NADH channel. By exploiting the 3D information in multiphoton image stacks, it is possible to simultaneously score the epithelial anomaly at the tissue surface (category C). Additionally, the number, as well as shape of cells in the stroma are quantified by categories E and F. The collagen matrix in the stroma, based on the label-free SHG channel is described by category D. For scoring, the image contrast of each multicolor 3D stack was adjusted manually upon visual inspection using Fiji, and scoring was performed separately and took a few seconds per stack. Example images for each

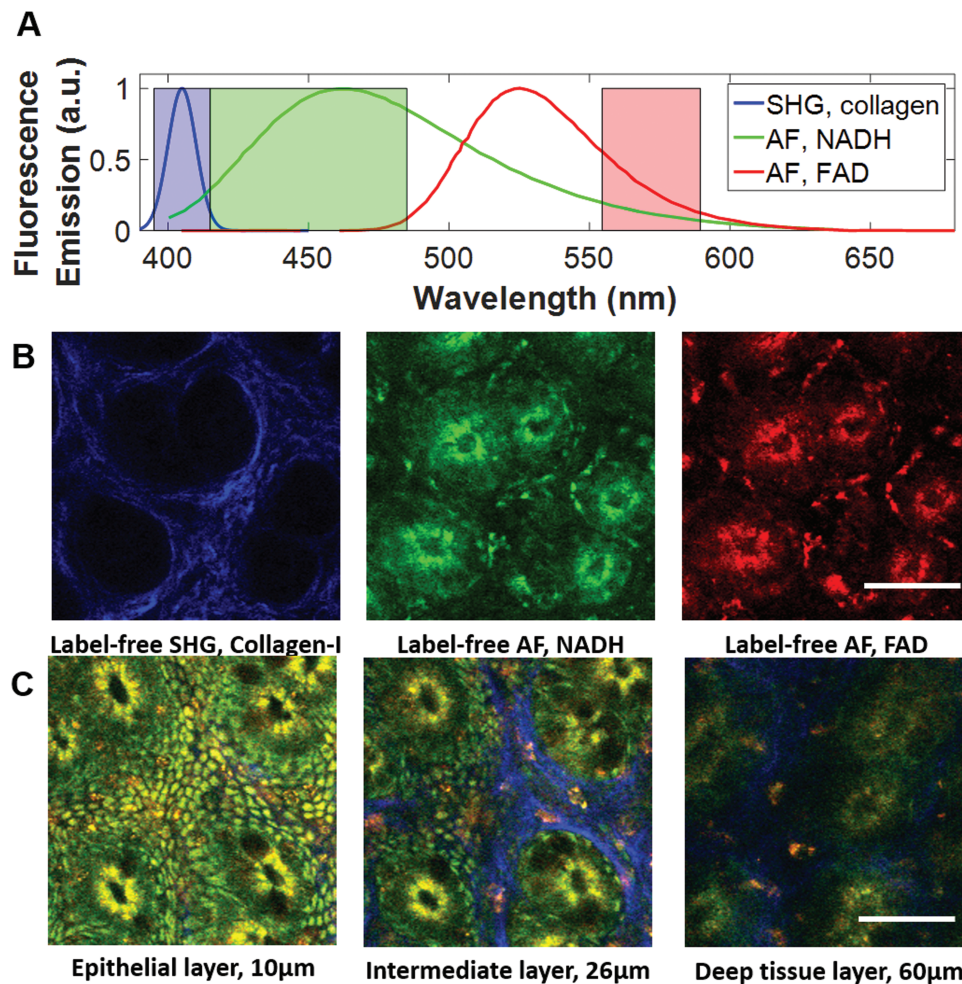


Figure 1. Label-free multiphoton microscopy (MPM) for 3-dimensional analysis of native tissues based on molecular specificity. A, The label-free signal is based on second harmonic generation (SHG) from collagen fibers, as well as on the natural autofluorescence (AF) from the cellular proteins nicotinamide adenine dinucleotide (NADH) and flavin adenine dinucleotide (FAD). B, Label-free MPM of fresh healthy murine colon tissue. From left to right, SHG from collagen fibers and AF signal from NADH and FAD. C, MPM is ideal for deep tissue imaging and can be used to record 3-dimensional image stacks. Scale bar = 50 μm .

of these categories are displayed in [Supplementary Figure 2](#). This MCS has already been applied to a preliminary analysis of in vivo data using MPEM.¹³ Compared with that initial study, we have now refined the wording of the score definitions to allow a more general usage of the MCS. In this study, we present a much more detailed analysis of this score from several different colitis models using label-free multiphoton imaging from ex vivo samples. Each label-free MPM image stack from ex vivo tissue samples of the different models has been scored. For a pathological comparison between different colitis models, the total MCS as sum of all 6 categories value was used. Statistical significance was tested by the Wilcoxon rank sum test (ranksum, MATLAB 2019; The MathWorks). Moreover, the average values for each individual category were visualized as spider plots to further identify differences between the different models.

Variability of the MCS Across Different Time Points, Different Observers, and Different Tissue Segments

To investigate the potential effect of degradation of fresh samples within the relevant time window of measurement,

one sample was placed at the microscope for 9 hours at room temperature and the exact same location was imaged every 2 hours (see [Supplementary Figure 3A](#)). In similar fashion, 3 samples from Rag1^{-/-} mice were imaged every 2 hours and scored via the MCS at every time point (see [Supplementary Figure 3B](#)). These samples were kept at 5°C between measurements. Apart from this variability analysis, only the data from the very first time point (2 hours after extraction) were used as Rag1^{-/-} control group.

Furthermore, the variability between different segments was evaluated based on the dataset of 42 MPM image stacks from 5 B6/J control animals and 21 stacks from 4 mice with acute DSS colitis. Here, the datasets were grouped and analyzed according to the location of the segment (see [Supplementary Figure 4](#)).

Finally, the same matched data described previously ($n_{\text{control}} = 42$ stacks, $n_{\text{DSS}} = 21$ stacks) were used to evaluate MCS variability between 2 different observers. All image stacks were scored by 2 different observers ([Supplementary Figure 5](#)). Cohen's kappa²² as well as accuracy were used as quality parameters to judge the level of agreement between both observers.

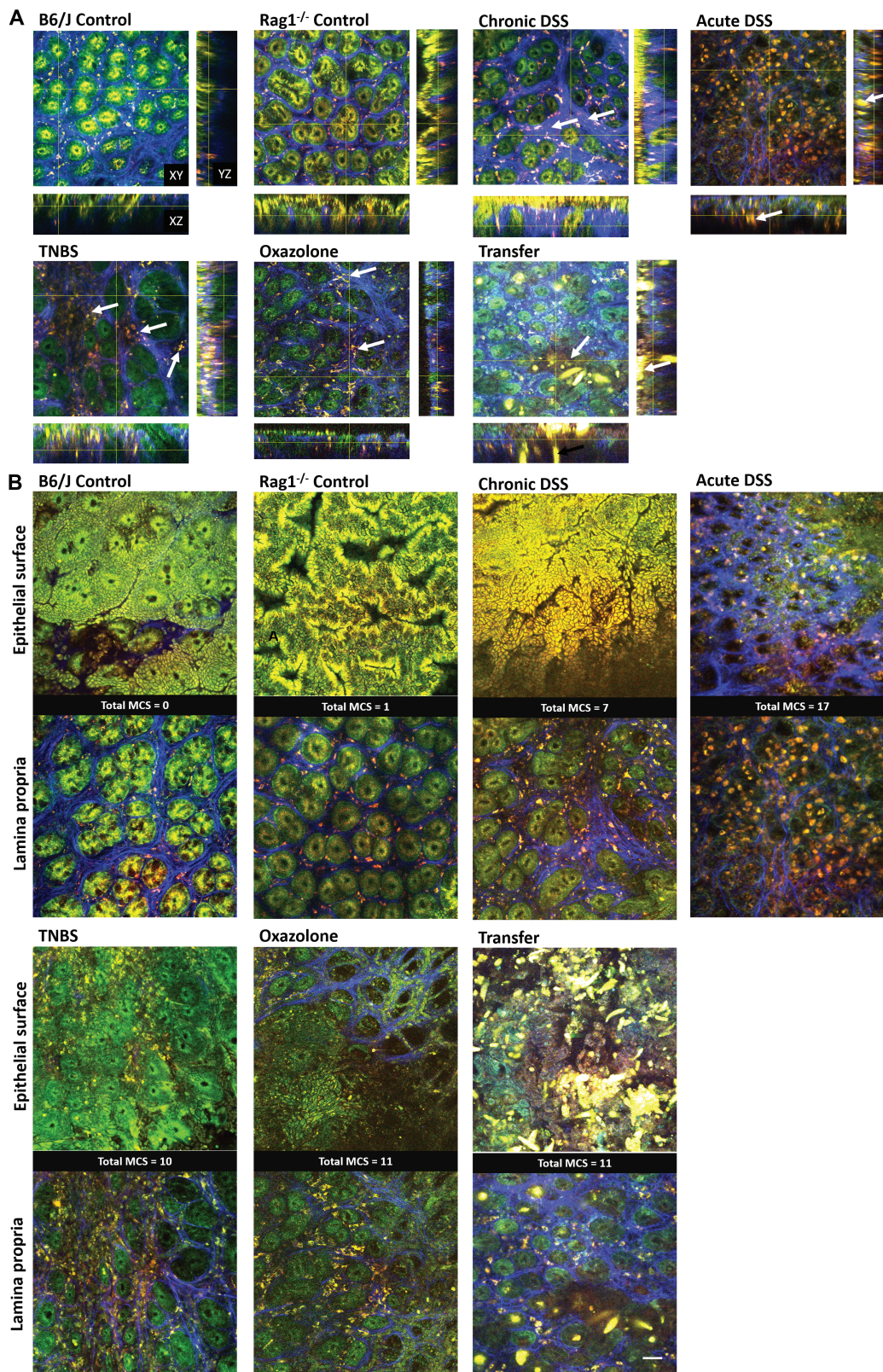


Figure 2. A, 3-dimensional label-free MPM image stacks in each of the investigated groups shown as X-Y, X-Z, and Y-Z representations. X-Y images are $400 \times 400 \mu\text{m}^2$, and white arrows indicate local clusters of immune cells in images of inflamed tissues. These clusters are not observed in healthy control samples. B, Label-free multiphoton microscopy enables microscopic evaluation of tissue morphology based on native signals. Representative images of epithelial layer (first row in each model) and lamina propria (second row in each model) in colon tissue from the same location and the same field of view. For each case, the multiphoton colitis score (MCS) value for the respective image stack is stated in the black text box. Seven groups were investigated: healthy colon (from B6/J and Rag1^{-/-} mice) and tissue samples from mice subjected to experimental colitis (acute and chronic DSS colitis, acute TNBS, oxazolone, and transfer colitis model). The second harmonic generation signal from collagen fibers is displayed in blue, autofluorescence from nicotinamide adenine dinucleotide in green and from flavin adenine dinucleotide in red. All images are $400 \times 400 \mu\text{m}^2$ (See online version for color figure).

Table 1. Definitions of the scoring categories in the MCS

Category	0	1	2	3
A: Crypt shape	Crypts are circular and symmetric and show an empty lumen in the center	Crypts show asymmetry, elongation, or shape that is not circular (slight deformations)	Crypt structure is deformed, still detectable in some locations; other locations show no crypts	Large areas (over 50% of the total image area) without detectable crypt structure
B: Crypt size and distance	Uniform size and distance of crypts	Size of or distance between crypts is not uniform	Size of and distance between crypts is not uniform	Average distance between crypts is larger than the diameter of 3 crypts
C: Epithelial anomaly	Closed surface, single epithelial cells visible, regular crypt openings, no additional voids or breaches, no stromal cells	Discontinuous surface, single epithelial cells visible, crypt openings are asymmetric, no stromal cells	Interrupted epithelial layer, holes, and breaches (openings do not end in crypts, a few stromal cells are visible)	Chaotic, destroyed structure, no regular pattern and/or increased stromal cellularity in epithelial layer
D: Collagen structure	Matrix intact, collagen around confined borders of all crypts, following regular crypt pattern	Matrix intact, collagen around confined borders of some crypts	Chaotic branching in some locations, confined borders of collagen around crypt in other locations	Chaotic branching of collagen in more than 50% the frame. Scar formation as bulk collagen accumulation
E: Cell shape and size in stroma	Cells in stroma are uniform in size and shape	Local variance in size or cell shape (eg, local clusters with similar-sized cells)	Local variance in size and cell shape; clusters of cells, including increased cell sizes	Severe variance in cell size and shape
F: Cellularity in stroma	Uniform and low cellularity; intracellular space in stroma extends over 5 cells	Cellularity locally increased in below 50% of the frame, where intracellular space extends over 3 cells	Cellularity generally increased in more than 50% of the frame	Cellularity globally increased in the entire frame; intracellular space below 4 cells

Correlation Between Label-Free MCS and Conventional H&E Scoring

To evaluate the performance of label-free MPM and the MCS in a direct comparison with conventional H&E assessment, H&E sections from the same animals were collected and imaged wherever possible. These H&E images were randomized and blinded for evaluation by an experienced pathologist. Global severity was graded according to a previously established H&E scoring system, ranging from 0 (no disease) to 10 (most severe disease).¹⁴ Detailed criteria contributing to this score are shown in [Supplementary Table 2](#). Thereafter, the total H&E score was determined for each individual animal as the average value over all images from the respective specimen. In the same fashion, all MPM image stacks from the same animal were averaged for the correlation analysis. H&E images from 2 animals with chronic colitis were judged as hyperplasia without cylindrical epithelial and were therefore excluded from the correlation analysis.

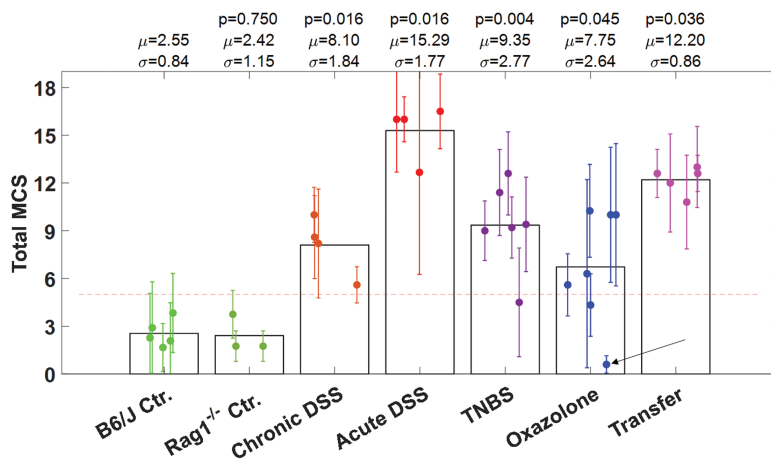
The averaged colitis score values for H&E and MCS were directly correlated, and a linear regression model was generated (see [Figure 3](#)). A threshold value for the H&E score was defined by the pathologist (cutoff = 2.5). Animals with a total H&E score below 3 were regarded as healthy, while animals with a score above were diagnosed as colitis. Accordingly, a cutoff for the MCS was defined as the value of 5. This value was deliberately chosen to split the total scoring range into the same ratio as the pathological H&E threshold (the lower third of the scoring range defines healthy and the upper two-thirds defines colitis). The respective diagnoses for healthy or colitis of the H&E score and the MCS were then compared in a confusion matrix for classification. The R^2 value was considered as quality parameter for the linear regression, while Cohen's kappa and accuracy served as quality parameters for the confusion matrix.

Results

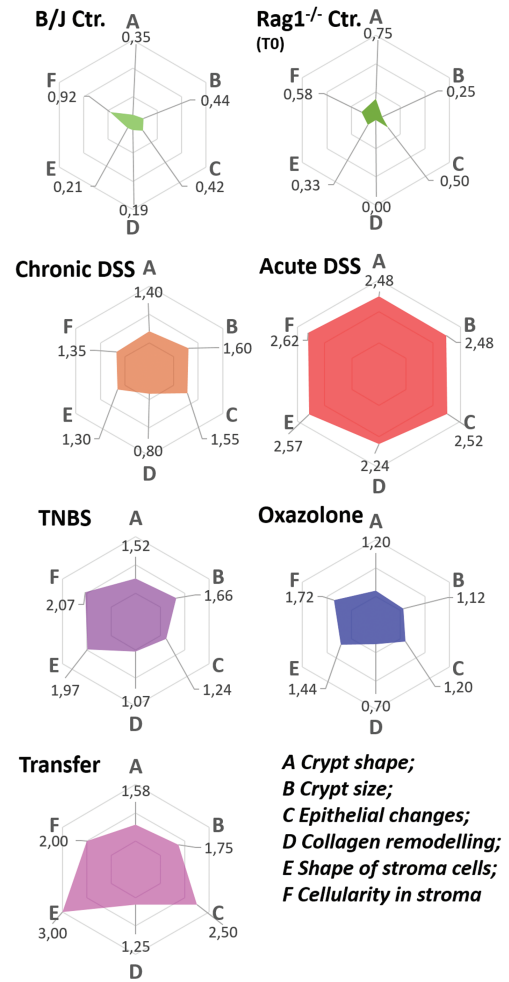
In this study, we quantify disease activity in different experimental colitis models using label-free MPM from fresh, ex vivo tissue samples and the new MCS. In this label-free optical microscopy technique, imaging contrast is generated from the natural autofluorescence in the spectral range of NADH and FAD, as well as from the SHG signal that is specific to molecular structures that lack inversion symmetry, such as collagen (see [Figure 1A](#)).⁴ In contrast to the elaborate tissue sectioning and staining protocol of H&E histology, MPM allows imaging of native and unstained tissue samples at different depths in the tissue (see [Figure 1B, 1C](#)). Overall, MPM can visualize native colon morphology at cellular resolution, allowing evaluation and grading of crypt pattern, collagen fibers, and stromal cells.

By using label-free MPM, we show the identification of characteristic differences between 5 of the most common experimental colitis models and 2 different control groups. Owing to the naturally confocal nature of MPM, it is particularly well suited for imaging 3D tissue samples, allowing X-Y, X-Z, and Y-Z representations, as shown in [Figure 2A](#) and in [Supplementary Video 1](#). This allows the simultaneous grading of the epithelial layer and lamina propria at the same location (see [Figure 2B](#)). Healthy control animals showed an intact epithelial layer and uniform pattern of round crypts, surrounded by regular collagen matrix. The number of cells in the stroma was low, and they were of uniform size. The acute DSS model showed erosion of both the epithelial layer and underlying crypt structures. The cellularity in the stroma was generally increased, and scar formation could be observed. In the case of chronic DSS colitis, erosion of epithelial cells was less apparent. Deep excavations were observed, reaching from the epithelial layer into the lamina propria. Crypts showed large variances in size and the cellularity

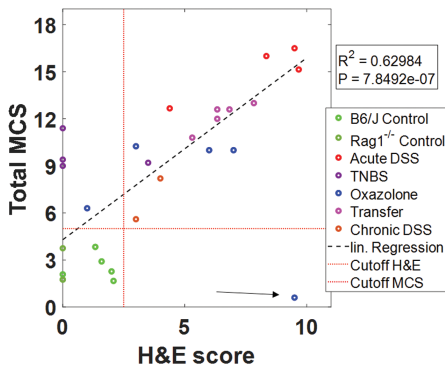
A) MCS in different colitis models



B) Differences in MCS categories



C) Correlation of MCS with H&E



D) Confusion matrix

		H&E	
		Colitis	Healthy
MCS	Colitis	100.0% 15	33.3% 4
	Healthy	0.0% 0	66.7% 8

Accuracy = 85.2%, $\kappa = 0.69$

Figure 3. The multiphoton colitis score (MCS) enables differentiation between healthy murine tissue samples and mice with colitis. A, Total MCS for different colitis models. Each dot represents an individual 3-dimensional image stack; the bar represents the mean value over all animals; *P* value compared with control animals and mean (μ) and SD (σ) of the entire group are shown as text. In the case of transfer colitis, significance was tested against the Rag1^{-/-} control group. Single data points represent mean MCS values of each individual animals, the error bar shows the SD of each mouse. One single animal in oxazolone colitis (arrow) was removed from mean calculation as statistical outlier. The dotted red line shows the diagnostic threshold for colitis (MCS = 5). B, Spider plots showing specific morphological parameters of the different colitis models, as quantified by the individual categories based on crypt shape and size, epithelial changes, collagen structure, shape, and cellularity in stroma cells. Each value is the mean over all image stacks in that group. C, Direct correlation between MCS from label-free multiphoton microscopy image stacks and the reference hematoxylin and eosin (H&E) score. Samples without H&E values have been removed. Each data point represents the averaged total score from 1 animal. A linear regression model was carried out and *R*² was deduced as quality parameters. As before, 1 outlier (arrow) was removed for regression and confusion matrix. The red dotted line represents the threshold values for H&E (2.5) and MCS (5). D, Confusion matrix of the diagnosis deduced from H&E scores compared with the respective diagnosis of label-free multiphoton microscopy. DSS, dextran sulfate sodium (See online version for color figure).

was locally increased. The TNBS model was characterized by increased cellularity in the stroma. The epithelial layer and crypt pattern remained mostly intact. Collagen structure changes were not observed in this model. However, it can be noted that the signal intensity from NADH in crypts was reduced. The acute oxazolone model revealed a specific disease pattern (ie, of increased cellularity in the stroma and an intense FAD signal in parts of the stromal tissue that were not localized to cells, but rather to vessels). The transfer colitis model showed an intact epithelial layer and mostly regular crypt pattern, with no collagen structure changes. Strikingly, transfer colitis showed larger cells with very high autofluorescence intensity (NADH and FAD) throughout all tissue layers.

These differences were quantified according to the MCS, which is subdivided into 6 categories with values between 0 and 3 (see Table 1). Each image stack was scored upon visual inspection, as shown in Figure 2B. The total MCS (sum of all categories) in each model was above the chosen diagnostic threshold of 6 (Figure 3A), within the variability between different image stacks of the same animal (error bars) and the variability between different animals in the same group. The difference between a given group and the control group reach statistical significance for each colitis model. Most morphological changes are predominant during acute DSS colitis (15.3 ± 1.7), followed by transfer colitis (12.2 ± 0.86). Chronic DSS colitis (8.1 ± 1.8), TNBS colitis (9.3 ± 2.7), and oxazolone colitis (7.7 ± 2.6) scored intermediately, and the

MCS in B6/J control animals (2.5 ± 0.8) and Rag1^{-/-} control animals (2.4 ± 1.2) was apparently lower.

Systematic differences between the models were quantified (Figure 3B), and the MCS of the control group remained below a value of 1 in all categories. The data from acute DSS colitis showed all categories at an average around 2.5. Chronic DSS colitis shows intermediate values in all categories (range, 1.3-1.7). Only the category for collagen structure is milder ($D = 0.8$). TNBS colitis shows intermediate values (range, 1.1-1.7) for categories A to E and an increased value for cellularity ($F = 2.07$). As already mentioned, the oxazolone model shows increased values only in the stromal cells categories ($E = 1.4$, $F = 1.7$). Finally, transfer colitis showed intermediate collagen structure changes scored as 1.2 but higher values for crypt pattern ($A = 1.5$ and $B = 1.7$). Transfer colitis showed a unique feature of very high autofluorescence (NADH and FAD) throughout all tissue layers, quantified as high values for epithelial anomalies (C), cellularity in the stroma (F), and a maximal value of 3.0 in shape of stromal cells (E). The MCS quantification was further validated by a direct comparison to H&E scoring according to the visual analog scale.¹⁴ Therefore, MCS values of all images from each animal were averaged. Accordingly, the average total visual analog scale score was deduced and both values were correlated (see Figure 3C). Based on the previously defined diagnostic thresholds for MCS and H&E score, a confusion matrix was generated (see Figure 3D). One single animal of the oxazolone model was regarded as outlier (arrow) and excluded from further analysis using the regression and confusion matrix. The data show very high correlation ($R^2 = 0.63$), and the confusion matrix indicates substantial agreement (85.2%; Cohen's $\kappa = 0.69$) between average label-free MCS and conventional H&E score.

Discussion

Endoscopic assessment of mucosal healing is the clinical gold standard for monitoring of IBD.²³ However, there is increasing evidence that evaluation of microscopic tissue structures offers additional diagnostic potential, as shown by H&E histology from patients with ulcerative colitis (UC).^{23,24}

Although histology provides detailed microscopic information, it can be considered time consuming and often limited for longitudinal monitoring during IBD or experimental colitis. Techniques such as CLE¹⁻³ or endocytoscopy²⁵ allow in vivo tissue evaluation on microscopic scales but require artificial contrast agents. In this regard, label-free multiphoton imaging shows potential to resolve some of these limitations, as it is based on native contrast and naturally provides 3D information on microscopic tissue morphology. Label-free MPM was already used to investigate ex vivo tissues from IBD biopsies¹² and DSS-induced colitis,²⁶ as well as azoxymethane (AOM)-DSS-induced neoplasia.²⁶ Additionally, quantification of crypt morphology in SHG images was used for detection of dysplastic transformations.²⁷ Label-free imaging is especially interesting for in vivo applications, which has led to label-free MPEM⁵⁻¹¹ and was already demonstrated in longitudinal in vivo studies of animal models.¹³

In this work, we used ex vivo tissues for a reliable benchmark comparison of the new MCS to demonstrate that label-free MPM can effectively discriminate healthy colon tissue from samples of 5 of the most common colitis models for

IBD research. Owing to the multifactorial and patient-specific origin of IBD, these experimental models are indispensable for the fundamental research of individual facets of IBD without the large variabilities in patient cohorts. We show an identification of specific patterns of features for each model. Morphological changes of mucosal crypts and connective tissue as well as natural differences in autofluorescence of stromal cells revealed specific characteristics of the inflammatory pathway in each model. As shown by numerous endoscopic implementations of MPEM, this approach is translatable to in vivo studies. Here, the systematic grading of label-free 3D imaging by the new MCS will be an essential quantification tool for future studies.

In this study, we chose to analyze the most distal part of the colon, as this section is most accessible to endomicroscopy systems. However, we also analyzed the variability between different segments from other parts of the colon in our supplementary material. Furthermore, the Supplementary Appendix shows that the variability of image quality and MCS values between 2 different observers and between different time points is much lower compared with intergroup differences between B6/J control animals and acute DSS colitis.

As described previously, we observed severe crypt loss, stromal cellularity, and collagen scar formation in DSS colitis. This is plausible because DSS treatment is known for inducing epithelial layer dysfunction and extensive immune cell infiltration.²⁰ Furthermore, DSS colitis was already used as reliable model for fibrosis.²⁸ We observed moderate crypt loss and stromal cell infiltration in chronic DSS colitis, where moderate immune cell activity²⁹ and epithelial remodeling²⁹ have been reported in previous studies. TNBS and oxazolone models are used to mimic either chronic Crohn's disease or UC, respectively,^{17,30} which is reflected by the increased intrastromal score of the MCS. Furthermore, TNBS was reported with modest changes in collagen matrix.³⁰ In contrast to that, the transfer colitis model is used to simulate the uncontrolled immune response in IBD patients. Our results on transfer colitis showed increased scores for cellularity in the stroma and disruptions in the epithelial layer, which might arise from commensal bacteria.³¹

Beyond the mere technological access to microscopic tissues, quantification of these features is essential. The Nancy score for H&E evaluation of UC includes features of colonic crypt loss, granulation tissue (chaotic blood vessels and neutrophils), and neutrophils as acute inflammatory infiltrates and lymphocytes as chronic inflammatory infiltrates.³² Respectively, we have now developed a systematic score for label-free multiphoton images. While this MCS cannot grade vascularity and does not differentiate between different types of immune cell, such as neutrophils and lymphocytes, it can nevertheless quantify crypt degradation and stromal cell infiltration. Label-free multiphoton imaging, as used in this study, already has demonstrated autofluorescence as biomarker for the distinction between adaptive (B cells, CD4⁺ T cells, CD8⁺ T cells) and innate immune cells (neutrophils, dendritic cells, macrophages).³³ In the future, we will exploit these differences in autofluorescence and combine them with morphological features like cell shape and size to develop a more specific separation of immune cells. Furthermore, the MCS grades pathological collagen structures and allows simultaneous grading

of epithelial layer and lamina propria because it is based on the specific SHG signal in 3D images. The overall diagnostic value of MCS, however, is comparable to H&E evaluation, which we confirmed by a direct validation (85.2% agreement) (Figure 3C, 3D).

Conclusions

In summary, we showed that label-free multiphoton imaging can differentiate unique inflammatory features in 5 of the most common experimental colitis models. We established an in-depth quantification of these features via the new MCS, which shows similar diagnostic yield as H&E scores. Label-free multiphoton imaging and the MCS provide complementary features that are not accessible by H&E. For longitudinal in vivo monitoring, H&E is usually not feasible, while label-free MPM and the MCS were already demonstrated for in vivo studies.¹³ According to the 3R principle, this approach effectively reduces the total number of specimen and refines data quality by allowing longitudinal monitoring in the same animal. Other in vivo technologies, such as CLE or endocytoscopy, do not allow detailed grading of inflammatory features and are still based on artificial contrasts. In the future, clinical translation of MPM could enable accurate differentiation of IBD subtypes or evaluation of therapeutics via label-free in vivo endomicroscopy.

Supplementary data

Supplementary data is available at *Inflammatory Bowel Diseases* online.

Acknowledgments

The authors gratefully acknowledge funding by the Deutsche Forschungsgemeinschaft (German Research Foundation).

Author contributions

O.-M.T. and L.K. as well as S.S. and M.J.W. contributed equally to this work and wrote the manuscript together. L.K. performed ex vivo multiphoton imaging of all native colon samples, analyzed the generated 3-dimensional image stacks, applied the MCS to MPM images, and performed data analysis of MCS and H&E score as well as statistical analysis and designed the figures. O.M.-T. supervised handling of mice samples from all models, performed histological staining and imaging of fixed tissue, and managed the models of acute and chronic DSS and TNBS colitis as well as transfer colitis. S.L. performed MPM imaging of the oxazolone model. K.L. provided the oxazolone model. T.K. provided the transfer model. K.S. supported the analysis of endoscopy data. C.H. provided unused samples of a chronic azoxymethane(AOM)-DSS model. L.K. and A.-L.M. analyzed sample degradation over time. L.K., A.D., B.C., and M.V. developed the MCS. M.V. scored the H&E reference images and served as second observer for MCS. B.W., C.N., K.H., M.V., M.F.N., O.F., S.S., and M.J.W. helped with data interpretation, discussion, and reading of the manuscript. L.K., O.-M.T., S.S., and M.J.W. designed the study and supervised all work.

Funding

This work was supported by the Deutsche Forschungsgemeinschaft (DFG) (German Research Foundation) project TRR241 (subproject C01 to S.S. and M.J.W.; A08 to K.H. and C.N.; C04 to M.N.). The work was supported by the Erlangen Graduate School in Advanced Optical Technologies within the framework of the German excellence initiative of the DFG, as well as by the Emerging Talents Initiative of the Friedrich-Alexander University Erlangen-Nürnberg (grant 2021-2_Tech_04_Kreiss to L.K.).

Conflicts of Interest

The authors declare no conflicts of interest.

References

- Goetz M, Ziebart A, Foersch S, et al. In vivo molecular imaging of colorectal cancer with confocal endomicroscopy by targeting epidermal growth factor receptor. *Gastroenterology*. 2010;138:435–446.
- Kiesslich R, Burg J, Vieth M, et al. Confocal laser endoscopy for diagnosing intraepithelial neoplasias and colorectal cancer in vivo. *Gastroenterology*. 2004;127:706–713.
- Kiesslich R, Duckworth CA, Moussata D, et al. Local barrier dysfunction identified by confocal laser endomicroscopy predicts relapse in inflammatory bowel disease. *Gut*. 2012;61:1146–1153.
- Zipfel WR, Williams RM, Webb WW. Nonlinear magic: multiphoton microscopy in the biosciences. *Nat Biotechnol*. 2003;21:1369–1377.
- Bao H, Allen J, Pattie R, et al. Fast handheld 2-photon fluorescence endoscope with a 475 μm x 475 μm field of view for in vivo imaging. *Opt Lett*. 2008;33:1333–1335.
- Dilipkumar A, Al-Shemmary A, Kreiß L, et al. Label-free multiphoton endomicroscopy for minimally invasive in vivo imaging. *Adv Sci (Weinh)*. 2019;6:1801735.
- Ducourthial G, Leclerc P, Mansuryan T, et al. Development of a real-time flexible multiphoton microendoscope for label-free imaging in a live animal. *Sci Rep*. 2015;5:18303.
- Liang W, Hall G, Messerschmidt B, Li MJ, Li X. Nonlinear optical endomicroscopy for label-free functional histology in vivo. *Light Sci Appl*. 2017;6:e17082.
- Llewellyn ME, Barretto RP, Delp SL, Schnitzer MJ. Minimally invasive high-speed imaging of sarcomere contractile dynamics in mice and humans. *Nature*. 2008;454:784–788.
- Myaing MT, MacDonald DJ, Li X. Fiber-optic scanning 2-photon fluorescence endoscope. *Opt Lett*. 2006;31:1076–1078.
- Rivera DR, Brown CM, Ouzounov DG, et al. Compact and flexible raster scanning multiphoton endoscope capable of imaging unstained tissue. *Proc Natl Acad Sci U S A*. 2011;108:17598–17603.
- Schürmann S, Foersch S, Atreya R, et al. Label-free imaging of inflammatory bowel disease using multiphoton microscopy. *Gastroenterology*. 2013;145:514–516.
- Kreiss L, Thoma O-M, Dilipkumar A, et al. Label-free in vivo histopathology of experimental colitis via 3-channel multiphoton endomicroscopy. *Gastroenterology*. 2020;159:832–834.
- Koelink PJ, Wildenberg ME, Stitt LW, et al. Development of reliable, valid and responsive scoring systems for endoscopy and histology in animal models for inflammatory bowel disease. *J Crohns Colitis*. 2018;12:794–803.
- Okayasu I, Hatakeyama S, Yamada M, et al. A novel method in the induction of reliable experimental acute and chronic ulcerative colitis in mice. *Gastroenterology*. 1990;98:694–702.
- Neufert C, Becker C, Neurath MF. An inducible mouse model of colon carcinogenesis for the analysis of sporadic and inflammation-driven tumor progression. *Nat Protoc*. 2007;2:1998–2004.

17. Hoffmann JC, Pawlowski NN, Grollich K, et al. Gammadelta T lymphocytes: a new type of regulatory T cells suppressing murine 2,4,6-trinitrobenzene sulphonic acid (TNBS)-induced colitis. *Int J Colorectal Dis.* 2008;23:909–920.
18. Boirivant M, Fuss IJ, Chu A, Strober W. Oxazolone colitis: a murine model of T helper cell type 2 colitis treatable with antibodies to interleukin 4. *J Exp Med.* 1998;188:1929–1939.
19. Heller F, Fuss IJ, Nieuwenhuis EE, et al. Oxazolone colitis, a Th2 colitis model resembling ulcerative colitis, is mediated by IL-13-producing NK-T cells. *Immunity.* 2002;17:629–638.
20. Eichele DD, Kharbanda KK. Dextran sodium sulfate colitis murine model: An indispensable tool for advancing our understanding of inflammatory bowel diseases pathogenesis. *World J Gastroenterol.* 2017;23:6016–6029.
21. Goldberg IG, Allan C, Burel JM, et al. The Open Microscopy Environment (OME) Data Model and XML file: open tools for informatics and quantitative analysis in biological imaging. *Genome Biol.* 2005;6:R47.
22. Cohen's kappa: compute the Cohen's kappa ratio on a 2x2 matrix. MATLAB Central File Exchange; 2007. Accessed 8 December 2021.
23. Neurath MF, Travis SP. Mucosal healing in inflammatory bowel diseases: a systematic review. *Gut.* 2012;61:1619–1635.
24. Bryant RV, Burger DC, Delo J, et al. Beyond endoscopic mucosal healing in UC: histological remission better predicts corticosteroid use and hospitalisation over 6 years of follow-up. *Gut.* 2016;65:408–414.
25. Neumann H, Fuchs FS, Vieth M, et al. Review article: in vivo imaging by endocytoscopy. *Aliment Pharmacol Ther.* 2011;33:1183–1193.
26. Makino T, Jain M, Montrose DC, et al. Multiphoton tomographic imaging: a potential optical biopsy tool for detecting gastrointestinal inflammation and neoplasia. *Cancer Prev Res (Phila).* 2012;5:1280–1290.
27. Prieto SP, Reed CL, James HM, et al. Differences in colonic crypt morphology of spontaneous and colitis-associated murine models via second harmonic generation imaging to quantify colon cancer development. *BMC Cancer.* 2019;19:428.
28. Scheibe K, Kersten C, Schmied A, et al. Inhibiting interleukin 36 receptor signaling reduces fibrosis in mice with Chronic intestinal inflammation. *Gastroenterology.* 2019;156:1082–1097.e11.
29. Taghipour N, Molaei M, Mosaffa N, et al. An experimental model of colitis induced by dextran sulfate sodium from acute progresses to chronicity in C57BL/6: correlation between conditions of mice and the environment. *Gastroenterol Hepatol Bed Bench.* 2016;9:45–52.
30. Antoniou E, Margonis GA, Angelou A, et al. The TNBS-induced colitis animal model: an overview. *Ann Med Surg (Lond).* 2016;11:9–15.
31. Aranda R, Sydora BC, McAllister PL, et al. Analysis of intestinal lymphocytes in mouse colitis mediated by transfer of CD4+, CD45RBhigh T cells to SCID recipients. *J Immunol.* 1997;158:3464–3473.
32. Marchal-Bressenot A, Scherl A, Salleron J, Peyrin-Biroulet L. A practical guide to assess the Nancy histological index for UC. *Gut.* 2016;65:1919–1920.
33. Lemire S, Thoma O-M, Kreiss L, et al. Natural NADH and FAD autofluorescence as label-free biomarkers for discriminating subtypes and functional states of immune cells. *Int J Mol Sci.* 2022;23:2338.